Inorganic Chemistry

Article

pubs.acs.org/IC

Special $_{\infty}^{1}[OPb_2]$ Chains and $_{\infty}^{1}[O_2Pb_3]$ Ribbons Based on OPb_4 Anion-Centered Tetrahedra in $Pb_2(O_4Pb_8)(BO_3)_3Br_3$ and $Pb_2(O_8Pb_{12})(BO_3)_2Br_6$

Lingyun Dong,[†,‡] Shilie Pan,*[,†] Ying Wang,[†,‡] Hongwei Yu,[†,‡] Xiaoyu Dong,[†] Shujuan Han,[†] and Min Zhang*[,†]

[†]Key Laboratory of Functional Materials and Devices for Special Environments of CAS, Xinjiang Key Laboratory of Electronic Information Materials and Devices, Xinjiang Technical Institute of Physics & Chemistry of CAS, 40-1 South Beijing Road, Urumqi 830011, China

[‡]University of Chinese Academy of Sciences, Beijing 100049, China

Supporting Information

ABSTRACT: The structures of two new lead-containing oxyborate bromines, $Pb_2(O_4Pb_8)(BO_3)_3Br_3$ (**1**) and $Pb_2(O_8Pb_{12})(BO_3)_2Br_6$ (**2**), are determined by single-crystal X-ray diffraction for the first time. Both of them crystallize in the space group *C*2/*c* of the monoclinic crystal system. Although the two compounds have the same type of fundmental building units (FBUs), the OPb_4 anion-centered tetrahedra and BO_3 triangles, they exhibit different connection modes. Compound **1** consists of single $_{\infty}^{1}[OPb_2]$ chains, while compound **2** possesses $_{\infty}^{1}[O_2Pb_3]$ ribbons. Interestingly, large Br atoms profoundly influence the conformation of polyions based on the OPb_4 anion-centered tetrahedra, resulting in single $_{\infty}^{1}[OPb_2]$ chains linked up by finite zweier chains with four OPb_4 tetrahedra via the opposite edges in compound **1** and $_{\infty}^{1}[O_2Pb_3]$ ribbons with sequential condensation of OPb_2 chains in compound **2**. A detailed description of the effect of large Br atoms on the conformation of polyions is discussed. IR spectroscopy, UV−vis−NIR diffuse reflectance spectroscopy, and thermal analysis are also performed on the reported materials.

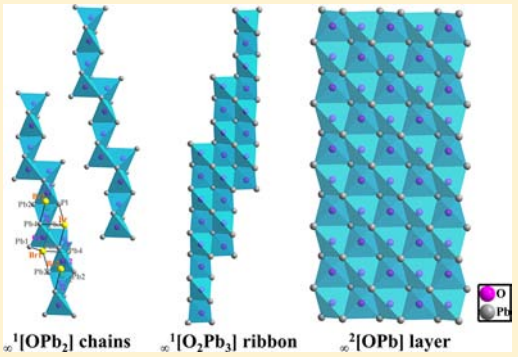

1. INTRODUCTION

The whole structures of inorganic compounds are commonly viewed based on the cation-centered polyhedra (CCP), which has been proven to be an efficient approach to analyze their structures as well as structure−property relationships.[1] Nevertheless, many inorganic compounds could be better treated as the construction of anion-centered tetrahedra (ACT), in which the most common anion is O^{2-}.[2] Structural subunits based on OA_4 with O as central atoms and A as ligands differ from those based on AO_4 cation-centered ones. The OA_4 tetrahedra may link through edges as well as through corners, and the bond valences between A and O are essentially higher than the bond valences between A and O atoms from other structural units.[3] More than that, the lead-containing oxysalts containing additional O atoms, which are not part of acid residues but are bonded exclusively to Pb^{2+},[4] are of great interest in the viewpoint of environmental chemistry,[5] ionic conductivity,[6] ferroelasticity,[7] and optical and optoelectronic properties.[8] In lead-containing oxysalts, the common ACT, OPb_4 tetrahedra, may condense by sharing edges and vertices to form polyions of different connectivity and dimensionality.[9] However, to the best of our knowledge, only two lead-containing borate bromines, $Pb_2B_5O_9Br$[10] and $Pb_6B_3O_{10}Br$,[11] have been synthesized in the $PbO−B_2O_3−PbBr_2$ system, and only several oxyborates containing OPb_4 tetrahedra, $Pb_4O(BO_3)_2$,[8b] and $Pb_6B_3O_{10}X$ (X = F, Cl, Br),[9a,11] in the $PbO−B_2O_3$ and $PbO−B_2O_3−PbX_2$ (X = halogen) systems. The O_3Pb_8 trimers exist in $Pb_4O(BO_3)_2$ and the isolated OPb_4 tetrahedra exist in $Pb_6B_3O_{10}X$ (X = F, Cl, Br) compounds. Until now, there is no report on the compounds containing chains or ribbons formed by edge-sharing OPb_4 tetrahedra in the $PbO−B_2O_3$ and $PbO−B_2O_3−PbX_2$ systems.[2a]

Within the systematic search of the lead-containing oxyborates, here we report two new oxyborates, $Pb_{10}B_3O_{13}Br_3$ and $Pb_{14}B_2O_{14}Br_6$. The edge-sharing OPb_4 tetrahedra exist in both compounds. In accord with Lima-de-Faria et al.[12] and Smith et al.,[13] the two crystal-chemical formulas, $Pb_2(O_4Pb_8)(BO_3)_3Br_3$ (**1**) and $Pb_2(O_8Pb_{12})(BO_3)_2Br_6$ (**2**), may be proposed for two compounds with anion-centered tetrahedra, which is helpful for understanding the whole structures directly. Interestingly, compound **1** consists of single $_{\infty}^{1}[OPb_2]$ chains in zigzag fashion. The serrated $_{\infty}^{1}[OPb_2]$ chains are linked up by finite linear zweier chains with four tetrahedra via the opposite edges. In comparison, compound **2** consists of serrated $_{\infty}^{1}[O_2Pb_3]$ ribbons with sequential condensation of OPb_2 chains. It should

Received: June 28, 2013
Published: September 19, 2013

   dx.doi.org/10.1021/ic401655h | *Inorg. Chem.* 2013, 52, 11377−11384

be noted that those chains and ribbons, which can be veiwed as derivatives from the $_{\infty}^{2}$[OPb] tetrahedral layer observed in tetragonal PbO compound, are rarely found in other lead-containing oxysalts, or even in other minerals and inorganic compounds. In addtition, Krivovichev et al.[14] discussed that the conformation of single edge-sharing OCu_4 tetrahedra chains can be interpreted as control of the large halide ions. However, the situation that two Br atoms are attached to the chain rotating the edge-sharing OPb_4 tetrahedra at the opposite direction has not been observed. In this article, the syntheses, structures, and properties of the two new compounds are described in detail. We also demonstrate that the large Br atoms significantly influence the conformation of polyions based on the OPb_4 tetrahedra of the reported materials.

2. EXPERIMENTAL SECTION

Reagents. PbO (Tianjin Damao Chemical Industry Co., Ltd., 99.5%), $PbBr_2$ (Aladdin Chemical Industry Co., Ltd., 99.0%), and H_3BO_3 (Tianjin HongYan Chemical Co., Ltd., 99.5%) are used as received.

Solid-State Synthesis. Polycrystalline samples of compounds **1** and **2** are synthesized by traditional solid-state reaction techniques. The starting chemicals are PbO, $PbBr_2$, and H_3BO_3. Separate stoichiometric mixtures of PbO, $PbBr_2$, and H_3BO_3 are initially ground well. The samples are placed in alumina crucibles and heated to 520 °C (540 °C for compound **2**), held for 3 d with several intermediate grindings, and then cooled to room temperature, respectively. The measured powder X-ray diffraction (XRD) patterns match the ones calculated from single-crystal XRD analysis very well, respectively (Figure 1). The powder diffraction data are then refined by Rietveld analysis with the program TOPAS.[15] The lattice parameters are a = 16.500, b = 8.952, c = 16.654 Å, and β = 114.384° for compound **1**, and a = 16.205, b = 8.921, c = 21.265 Å, and β = 97.781° for compound **2**, respectively.

Crystal Growth. Single crystals of two new compounds are obtained by high-temperature solution method.

Compound **1**. Reaction mixtures of PbO, $PbBr_2$, and H_3BO_3 at a molar ratio of 11:1:6, that is, PbO (11 mmol, 2.455 g), $PbBr_2$ (1 mmol, 0.367 g), and H_3BO_3 (6 mmol, 0.371 g), are ground carefully to homogeneity in an agate mortar, and then transferred to a platinum crucible. The platinum crucible is put into a vertical, programmable temperature furnace under air, and then the furnace is heated up to 630 °C and kept at this temperature for 12 h. After then, the furnace is cooled rapidly down to 500 °C and then slowly down to 420 °C at a rate of 3 °C/h, kept at a constant temperature, and then cooled down to room temperature at a rate of about 20 °C/h. Colorless and block-shaped crystals are found in the crucible.

Compound **2**. A mixture of PbO, $PbBr_2$, and H_3BO_3 at a molar ratio of 5.7:1:2, that is, PbO (17 mmol, 3.794 g), $PbBr_2$ (3 mmol, 1.101 g), and H_3BO_3 (6 mmol, 0.371 g), is loaded in a platinum crucible and heated in a vertical, programmable temperature furnace at 700 °C and kept at this temperature for 8 h. The homogenized solution is then cooled slowly (5 °C/h) to the final crystallization temperature (580 °C), followed by cooling to room temperature after the furnace is powered off. Yellow and block-shaped crystals of compound **2** are found in the crucible.

The crystals are manually selected for structural characterization by single-crystal XRD measurements and later determined as compounds **1** and **2**.

Structural Determinations. Block crystals of compounds **1** (0.066 mm × 0.077 mm × 0.136 mm) and **2** (0.066 mm × 0.083 mm × 0.182 mm) are used for single-crystal data collection. Data are collected on a Bruker SMART APEX II CCD diffractometer using monochromatic Mo Kα radiation (λ = 0.71073 Å) at 293(2) K and integrated with the SAINT-Plus program.[16] The numerical absorption corrections are carried out using the SADABS program for area detector.[17] All refinements are completed with programs from the SHELXTL-97 crystallographic software package.[18] The structures are solved by direct methods. All the atoms are refined using full matrix least-squares techniques with anisotropic thermal parameters. Final least-squares refinements are on F_o^2 with data having $F_o^2 \geq 2\sigma(F_o^2)$. In compound **1**, the occupancy factors of O6, O7, and O8 atoms are reduced to half of their original values because of their large thermal parameters as well as the requirement for charge balance.[19] The structures are checked for missing symmetry elements with PLATON,[20] and no additional symmetries are found, respectively. The crystal powder samples are prepared and irradiated by a Q-switched Nd:YAG solid-state laser (1064 nm, 10 kHz, 10 ns), respectively. There is no green light (frequency-doubled output) emitted from the samples, which further proves that both compounds are centrosymmetric.

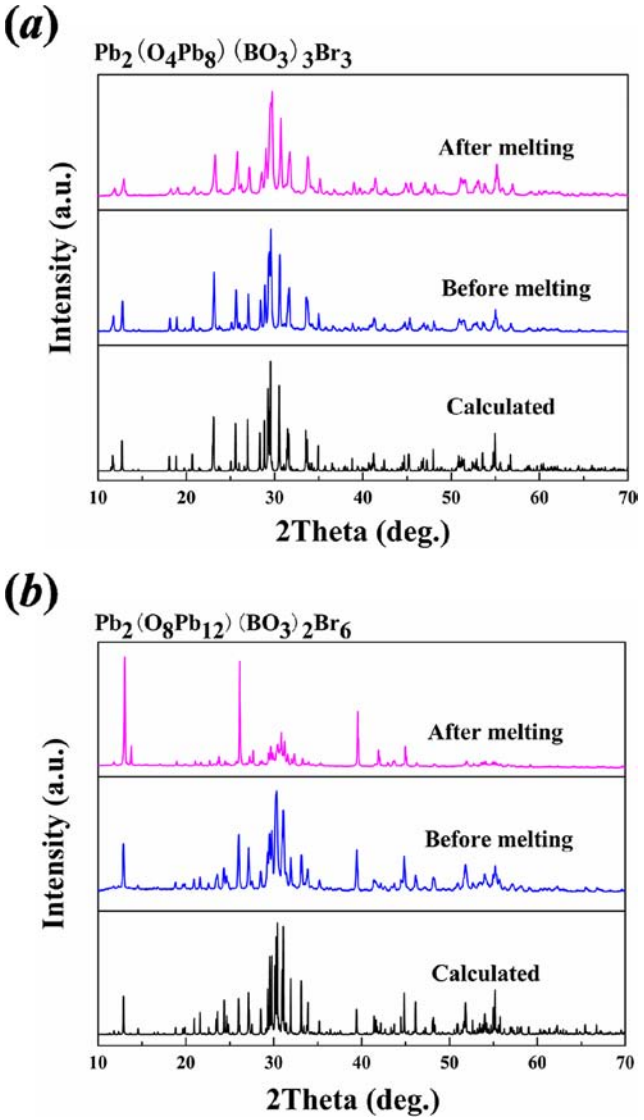

Figure 1. Experimental and calculated XRD patterns of (a) $Pb_2(O_4Pb_8)(BO_3)_3Br_3$ and (b) $Pb_2(O_8Pb_{12})(BO_3)_2Br_6$.

Relevant crystallographic data are listed in Table 1. The final atomic coordinates with equivalent isotropic displacements and bond valence analysis[21] for two new compounds are given in Table 2, and selected bond lengths are given in Table S1 in the Supporting Information. Further details of the crystal structure investigations may be obtained from the CIF files in the Supporting Information.

Infrared Spectroscopy. Infrared spectra of powder samples of compounds **1** and **2** are collected at room temperature on a Shimadzu IR Affinity-1 Fourier transform infrared spectrometer in the range of 400−4000 cm^{-1} at room temperature, with the samples embedded in

dx.doi.org/10.1021/ic401655h | Inorg. Chem. 2013, 52, 11377−11384

Table 1. Crystal Data and Structure Refinements for $Pb_2(O_4Pb_8)(BO_3)_3Br_3$ and $Pb_2(O_8Pb_{12})(BO_3)_2Br_6$

empirical formula	$Pb_2(O_4Pb_8)(BO_3)_3Br_3$	$Pb_2(O_8Pb_{12})(BO_3)_2Br_6$
formula weight	2552.06	3625.74
temperature (K)	296(2)	296(2)
wavelength (Å)	0.71073	0.71073
crystal system, space group	monoclinic, *C*2/*c*	monoclinic, *C*2/*c*
a (Å)	16.482(9)	16.197(2)
b (Å) *β* (deg)	8.947(5) 114.337(6)	8.9284(14) 97.882(9)
c (Å)	16.645(9)	21.278(3)
volume (Å^3)	2236(2)	3048.0(7)
Z, calculated density (mg/m^3)	4, 7.579	4, 7.901
F(000)	4176	5920
cryst size (mm^3)	0.066 × 0.077 × 0.136	0.066 × 0.083 × 0.182
limiting indices	$-19 \le h \le 21, -11 \le k \le 9, -21 \le l \le 15$	$-20 \le h \le 20, -11 \le k \le 11, -27 \le l \le 27$
reflections collected/unique	6670/2544	24517/3471
completeness to *θ* (deg, %)	27.43, 99.7	27.49, 99.4
data/restraints/parameters	2544/24/148	3471/24/166
goodness-of-fit on F^2	0.995	1.053
final *R* indices $[F_o^2 > 2\sigma(F_o^2)]^a$	$R_1 = 0.0395$, $wR_2 = 0.0741$	$R_1 = 0.0433$, $wR_2 = 0.1126$
R indices (all data)^a	$R_1 = 0.0610$, $wR_2 = 0.0819$	$R_1 = 0.0594$, $wR_2 = 0.1211$
largest diff. peak, hole (e·Å^{-3})	2.862 and −2.417	4.113 and −2.579

$^a R_1 = \Sigma||F_o| - |F_c||/\Sigma|F_o|$ and $wR_2 = [\Sigma w(F_o^2 - F_c^2)^2/\Sigma wF_o^4]^{1/2}$ for $F_o^2 > 2\sigma(F_o^2)$.

dried KBr matrixes, respectively (5 mg of the sample and 500 mg of KBr).

UV−Vis−NIR Diffuse Reflectance Spectroscopy. The Solid-Spec-3700DUV spectrophotometer is used to measure the spectra of powder samples of two compounds over a 190−2600 nm wavelength range at room temperature. Reflectance spectra are converted to absorbance with the Kubelka−Munk function, respectively.[22]

Thermal Behavior. The thermal properties of two compounds are studied on a NETZSCH STA 449C simultaneous analyzer under flowing of nitrogen gas. Compound **1** is heated from the room temperature to 670 °C and then allowed to cool to 200 °C at a rate of 5 °C/min, and compound **2** is heated from the room temperature to 800 °C at a rate of 5 °C/min, respectively.

3. RESULTS AND DISCUSSION

Crystal Structures. On the basis of single-crystal XRD analysis, both compounds crystallize in the monoclinic crystal system with the centrosymmetric space group *C*2/*c*.

*$Pb_2(O_4Pb_8)(BO_3)_3Br_3$ (**1**).* In the asymmetric unit, compound **1** consists of five crystallographically distinct Pb atoms, two B atoms, eight O atoms, and two Br atoms (Table 2). As shown in Figure 2a, the $_\infty^1[OPb_2]$ chains formed by edge-sharing OPb_4 tetrahedra (Figure 2b) are connected through the BO_3 triangles and the remaining Pb atoms to build the network with large channels, where the Br atoms are located. It is clear that the Br1 atoms are on the edge of the channels with the Pb−Br bond lengths from 3.296(29) to 3.715(32) Å, while the Br2 atoms are nearly in the middle of the channels with the Pb−Br bonds from 3.443(25) to 3.624(25) Å. Consequently, the bond valence sum for the Br2 atom is lower than that of the Br1 atom, which is typical for halogen anions located in structure cavities.[23] Two types of isolated BO_3 groups exist in compound **1** with the lengths of the B−O bonds from 1.33(3) to 1.49(2) Å. The O6, O6′, O7, O7′, O8, and O8′ atoms in $B2O_3$ groups are generated by the 2-fold axis, and the sites of these atoms are half-occupied. As shown in Figure S1 in the Supporting Information, the $B2O_3$ group randomly adopts an up orientation or a down orientation. Here, the up and down orientation of $B2O_3$ group is defined according to the relative position of the O6 atoms in the $B2O_3$ group along the [101] direction. In compound **1**, there are five types of distorted polyhedra (see Figure S2a in the Supporting Information), $Pb1O_nBr_m$ ($n = 4$, $m = 1, 2, 3$; $n = 5$, $m = 2$; $n = 6$, $m = 1$) polyhedra. The bond valence calculations for all of the Pb, B, and O atoms are reasonable.

*$Pb_2(O_8Pb_{12})(BO_3)_2Br_6$ (**2**).* Different from compound **1**, compound **2** features a layered structure (see Figure 3a). The $_\infty^1[O_2Pb_3]$ ribbons, which are also constructed by the edge-sharing OPb_4 (Figure 3b), are connected with the BO_3 triangles and the remaining Pb atoms form two-dimensional layers, while all the Br atoms are filled in the interlayers. Only one type of BO_3 triangle exists in compound **2** with the lengths of the B−O bonds from 1.36(2) to 1.39(2) Å. As seen in Figure 3a, the BO_3 triangles skew toward the *b*-axis and align antiparallel to the *a*-axis. There are seven types of Pb-centered polyhedra (see Figure S2b in the Supporting Information), $Pb1O_4Br_3$, $Pb2O_4Br_3$, $Pb3O_4Br_4$, $Pb4O_3Br_3$, $Pb5O_4Br_2$ $Pb6O_3Br_3$, and $Pb7O_2Br_3$ polyhedra.

There are also OPb_3B tetrahedra in both compounds (see Figure S3 in the Supporting Information). The connection modes of the OPb_3B tetrahedra in both compounds are similar, the OPb_3B tetrahedron is connected through edge or corner with its adjacent OPb_3B tetrahedra forming infinite $_\infty^1[OPb_3B]$ chains.

Comparison of the $_\infty^1[OPb_2]$ Chains and the $_\infty^1[O_2Pb_3]$ Ribbons. The $_\infty^1[OPb_2]$ chains in compound **1** and the $_\infty^1[O_2Pb_3]$ ribbons in compound **2** may be considered as derivatives of the continuous sheet of OPb_4 tetrahedra from the tetragonal modification of PbO compound (see Figure 4). However, those chains and ribbons described here, as far as we know, have not appeared in any other lead-containing oxysalts. As seen in Figure 2b, the single $_\infty^1[OPb_2]$ chain is constructed by finite linear zweier chains with four tetrahedra via the opposite edges in identity period forming a zigzag fashion. The conformation of the chains is controlled by the presence of relatively large Br atoms. Two Br1 atoms, each forming four Br−Pb bonds with the Pb atoms, are attached to the chain at the opposite position rotating the two pairs of edge-sharing OPb_4 tetrahedra. The other type of the Br2 atoms, which only

dx.doi.org/10.1021/ic401655h | Inorg. Chem. 2013, 52, 11377−11384

Table 2. Atomic Coordinates, Equivalent Isotropic Displacement Parameters (Å^2), and Bond Valence Sum for $Pb_2(O_4Pb_8)(BO_3)_3Br_3$ and $Pb_2(O_8Pb_{12})(BO_3)_2Br_6$

$Pb_2(O_4Pb_8)(BO_3)_3Br_3$							
atoms	Wyckoff positions	S.O.F.	*x*	*y*	*z*	*U*(eq)[a]	BVS
Pb1	8*f*	1	0.2787(1)	0.0450(1)	0.3980(1)	0.018(1)	1.846
Pb2	8*f*	1	0.6074(1)	0.5384(1)	0.5007(1)	0.018(1)	1.855
Pb3	8*f*	1	0.4770(1)	0.8469(1)	0.5636(1)	0.017(1)	1.908
Pb4	8*f*	1	0.4079(1)	0.7559(1)	0.3338(1)	0.018(1)	1.790
Pb5	8*f*	1	0.1565(1)	0.6784(1)	0.2943(1)	0.026(1)	1.918
B1	8*f*	1	0.6959(13)	0.5780(20)	0.6902(13)	0.020(4)	2.938
B2	4*c*	1	0.2500	0.7500	0.5000	0.022(6)	2.785
O1	8*f*	1	0.4131(8)	0.9577(12)	0.4264(8)	0.022(3)	1.906
O2	8*f*	1	0.4731(8)	0.6489(11)	0.4676(8)	0.021(3)	1.998
O3	8*f*	1	0.6429(7)	0.6738(12)	0.6267(8)	0.019(3)	1.951
O4	8*f*	1	0.2376(7)	0.8722(12)	0.2773(7)	0.022(3)	2.066
O5	8*f*	1	0.2930(7)	0.5664(12)	0.3324(9)	0.026(3)	1.985
O6	8*f*	0.5	0.1638(14)	0.7240(20)	0.4224(15)	0.018(5)	1.931
O7	8*f*	0.5	0.3122(16)	0.8430(20)	0.4896(16)	0.022(6)	1.831
O8	8*f*	0.5	0.2386(16)	0.8160(20)	0.4244(17)	0.025(6)	2.102
Br1	8*f*	1	0.6174(1)	0.8534(2)	0.3923(1)	0.033(1)	0.718
Br2	4*e*	1	0.5000	0.4573(3)	0.2500	0.048(1)	0.346
$Pb_2(O_8Pb_{12})(BO_3)_2Br_6$							
atoms	Wyckoff positions	S.O.F.	*x*	*y*	*z*	*U*(eq)[a]	BVS
Pb1	8*f*	1	0.3099(1)	0.0647(1)	0.4244(1)	0.014(1)	1.939
Pb2	8*f*	1	0.5327(1)	0.1523(1)	0.4465(1)	0.014(1)	1.917
Pb3	8*f*	1	0.3878(1)	0.4602(1)	0.4856(1)	0.014(1)	1.869
Pb4	8*f*	1	0.2295(1)	0.6655(1)	0.3533(1)	0.017(1)	1.791
Pb5	8*f*	1	0.5384(1)	0.2387(1)	0.6143(1)	0.014(1)	1.922
Pb6	8*f*	1	0.3856(1)	0.3654(1)	0.3167(1)	0.016(1)	1.717
Pb7	8*f*	1	0.1393(1)	0.2653(1)	0.2827(1)	0.018(1)	1.868
B1	8*f*	1	0.2835(12)	0.0036(19)	0.2840(9)	0.011(4)	2.949
O1	8*f*	1	0.4340(7)	−0.442(12)	0.4509(5)	0.010(2)	1.924
O2	8*f*	1	0.5158(7)	0.3455(12)	0.5181(6)	0.014(3)	1.959
O3	8*f*	1	0.3101(8)	−0.1037(13)	0.2500	0.3294(6)	1.916
O4	8*f*	1	0.3572(7)	0.5788(12)	0.3747(5)	0.013(2)	1.830
O5	8*f*	1	0.3976(8)	0.2611(12)	0.4108(6)	0.017(3)	1.927
O6	8*f*	1	0.2664(8)	0.1463(13)	0.3014(6)	0.019(3)	1.871
O7	8*f*	1	0.2714(8)	−0.0388(13)	0.2210(6)	0.020(3)	2.122
Br1	8*f*	1	0.1693(1)	0.3582(2)	0.4170(1)	0.019(1)	1.035
Br2	4*e*	1	0	0.5484(4)	0.2500	0.054(1)	0.244
Br3	4*c*	1	0.2500	0.7500	0.5000	0.021(1)	0.992
Br4	8*f*	1	0.5765(1)	0.4611(2)	0.3505(1)	0.024(1)	0.718

[a] *U*(eq) is defined as one third of the trace of the orthogonalized U_{ij} tensor.

form one Br−Pb bond with the Pb atom, do not play the role of rotation. Finally, the conformation of the single chain is serrated. Interestingly, the O_2Pb_3 ribbon in compound **2** can be seen as the sequential condensation of double OPb_2 chains in compound **1** (see Figure 4), then the O_2Pb_3 ribbons are linked via the opposite edges forming the $_\infty^1[O_2Pb_3]$ ribbons. From Figure 2a to Figure 3a, it is clear that the adjacent layers in compound **2** are connected with all the Br atoms, which are not connected with BO_3 groups like that in compound **1**. As shown in Figure 5, the arrangements of $B1O_3$ groups viewed in the (100) face are similar in both compounds. In Figure 5a, the adjacent $B1O_3$ groups in compound **1** skew toward the *b*-axis and align parallel to the *a*-axis, and the $B2O_3$ groups are between the adjacent antiparallel lines of the $B1O_3$ groups. However, there are only one type of $B1O_3$ groups in compound **2** arraying similarly to that in compound **1** (see Figure 5b). Obviously, from compound **1** to compound **2**, three Br atoms replace the $B2O_3$ groups, which means that from single $_\infty^1[OPb_2]$ chains to $_\infty^1[O_2Pb_3]$ ribbons, the space becomes large enough to locate the larger volume of three Br atoms instead of one BO_3 group. Consequently, compound **2** has a layered structure, but compound **1** has a network structure. In addition, the bond lengths of the additional O atoms (the O1 and O2 atoms in compound **1**, and the O1, O2, O4, and O5 atoms in compound **2**) with the Pb atoms are essentially shorter than that of the other O atoms with the Pb atoms (see Table S1 in the Supporting Information), which is typical for the oxysalts.[24]

Infrared Spectroscopy. Figure S4 in the Supporting Information presents the infrared spectra of compounds **1** and **2**. Referring to the literature,[25] the peaks at 1323, 1279, 1230, 1175, and 956 cm^{-1} for compound **1** and 1202 cm^{-1} for compound **2** can be assigned to the asymmetric stretching and symmetric stretching vibrations of BO_3, while the peaks located

dx.doi.org/10.1021/ic401655h | *Inorg. Chem.* 2013, 52, 11377−11384

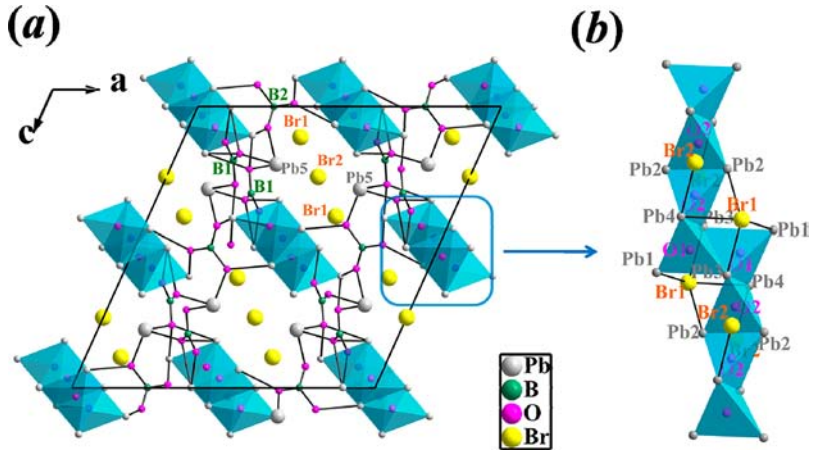

Figure 2. (a) Structure of $Pb_2(O_4Pb_8)(BO_3)_3Br_3$ viewed along the [010] direction. The blue units are the $_\infty^1[OPb_2]$ chains formed by edge-sharing OPb_4 tetrahedra; (b) the connectivity of finite linear zweier chains with four tetrahedra due to adaptation to Br atoms.

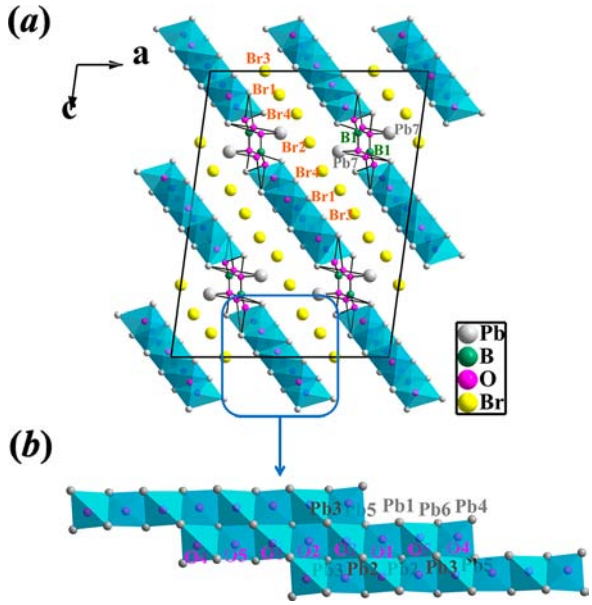

Figure 3. (a) Structure of $Pb_2(O_8Pb_{12})(BO_3)_2Br_6$ viewed along the [010] direction. The blue units are the $_\infty^1[O_2Pb_3]$ ribbons formed by edge-sharing OPb_4 tetrahedra; (b) the infinite $_\infty^1[O_2Pb_3]$ ribbons formed by continuous edge-sharing OPb_4 tetrahedra in $Pb_2(O_8Pb_{12})(BO_3)_2Br_6$ compound.

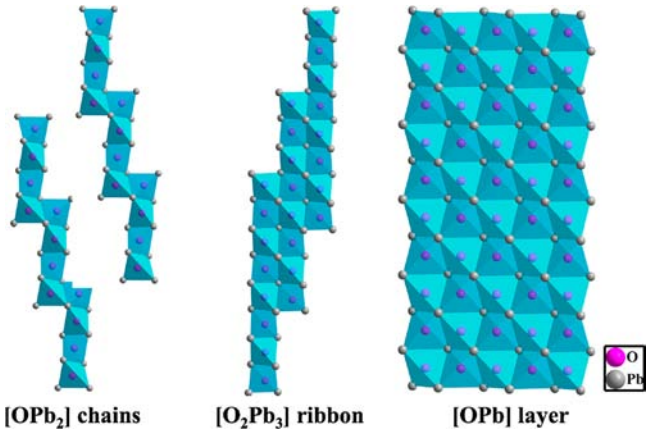

Figure 4. (a) Infinite $_\infty^1[OPb_2]$ chains formed by continuous edge-sharing OPb_4 tetrahedra in $Pb_2(O_4Pb_8)(BO_3)_3Br_3$ compound; (b) infinite $_\infty^1[O_2Pb_3]$ ribbons formed by continuous edge-sharing OPb_4 tetrahedra in $Pb_2(O_8Pb_{12})(BO_3)_2Br_6$ compound; (c) oxocentered tetrahedral layer formed by continuous linking of OPb_4 tetrahedra via edges in tetragonal PbO compound.

at 736, 709, and 615 cm^{-1} for compound **1** and 736, 709, and 610 cm^{-1} for compound **2** are likely to be from the out-of-plane bending of B−O in BO_3, respectively. The peaks at 577 and 418 cm^{-1} for compound **1** and 567 and 447 cm^{-1} for compound **2** are attributed to bending vibrations.

UV−Vis−NIR Diffuse Reflectance Spectroscopy. The UV−vis−NIR diffuse reflectance spectra of compounds **1** and **2** in the region 190−2600 nm are deposited in Figure 6. Absorption (K/S) data were calculated from the following Kubelka−Munk function:

$$F(R) = \frac{(1-R)^2}{2R} = \frac{K}{S}$$

with R representing the reflectance, K the absorption, and S the scattering. In their $F(R)$ versus E (eV) plots, the band gaps are 3.25 eV for compound **1** and 2.62 eV for compound **2**, which means that the absorption edges are about 382 nm for compound **1** and 473 nm for compound **2**, respectively. That is, the absorption edge of compound **1** is located in the UV region, while the absorption edge of compound **2** is located in the blue region, which are consistent with the colors of compounds **1** (colorless) and **2** (yellow).

Thermal Behavior. The TG-DSC (thermogravimetric differential scanning calorimetry) curves of two compounds are shown in Figure 7. The DSC curve of compound **1** exhibits one endothermic peak on the heating curve and one exothermic peak on the cooling curve, and there is no obvious weight loss in the TG curve, revealing that the compound melts congruently at around 645 °C (see Figure 7a). To verify that compound **1** melts congruently, the powders of compound **1** are placed into a platinum crucible and heated to 650 °C until the powders melt completely. The powders are then allowed to cool to room temperature. Analysis of the powder XRD patterns of the solidified melts reveals that the solid products exhibit a diffraction pattern identical to that of the initial compound powders (see Figure 1a), further demonstrating that compound **1** melts congruently. The DSC curve of compound **2** also exhibits one endothermic peak in the heating curve; however, the obvious weight loss was observed from the TG

dx.doi.org/10.1021/ic401655h | Inorg. Chem. 2013, 52, 11377−11384

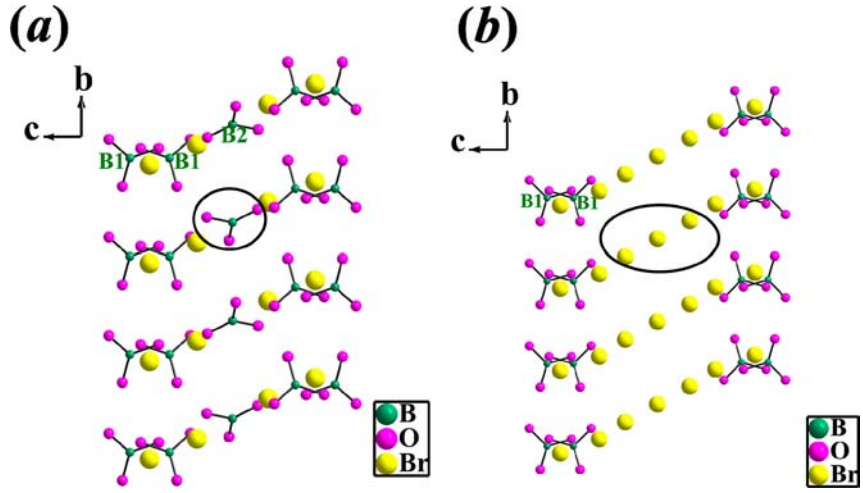

Figure 5. Arrangements of BO_3 groups with Br atoms in (a) $Pb_2(O_4Pb_8)(BO_3)_3Br_3$ and (b) $Pb_2(O_8Pb_{12})(BO_3)_2Br_6$ viewed along the [100] direction.

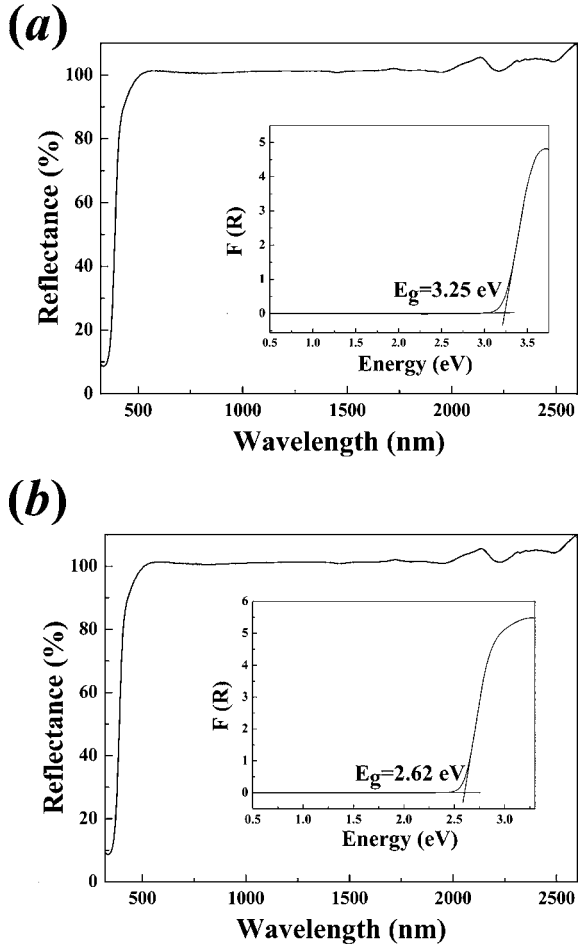

Figure 6. UV−vis−NIR diffuse reflectance spectra of (a) $Pb_2(O_4Pb_8)(BO_3)_3Br_3$ and (b) $Pb_2(O_8Pb_{12})(BO_3)_2Br_6$.

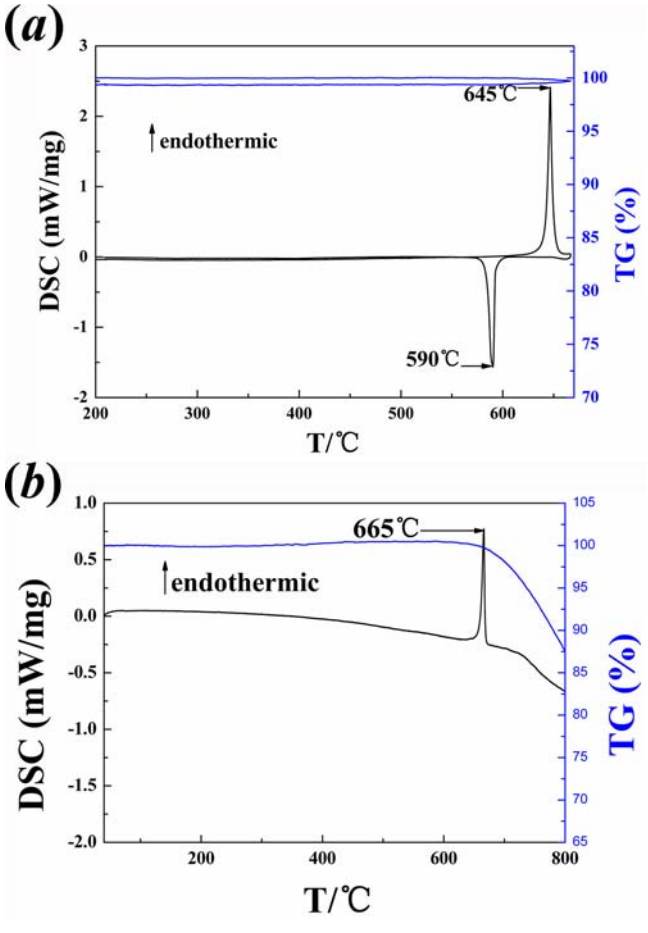

Figure 7. TG-DSC curves of (a) $Pb_2(O_4Pb_8)(BO_3)_3Br_3$ and (b) $Pb_2(O_8Pb_{12})(BO_3)_2Br_6$.

curve, revealing that compound **2** melts incongruently (see Figure 7b). After that, the compound **2** powders are heated to 665 °C, and then slowly cooled to room temperature. Analysis of the powder XRD patterns of the solidified melts reveals that the solid product exhibits a diffraction pattern different from that of the initial compound **2** powders (see Figure 1b), further demonstrating that compound **2** melts incongruently.

4. CONCLUSIONS

Two new lead-containing oxyborate bromines, $Pb_2(O_4Pb_8)(BO_3)_3Br_3$ (**1**) and $Pb_2(O_8Pb_{12})(BO_3)_2Br_6$ (**2**), have been synthesized. The single-crystal XRD analysis shows that both of them crystallize in the space group *C*2/*c* of the monoclinic crystal system. The single $_\infty^1[OPb_2]$ chains in compound **1** and the $_\infty^1[O_2Pb_3]$ ribbons in compound **2** formed by edge-sharing

dx.doi.org/10.1021/ic401655h | *Inorg. Chem.* 2013, 52, 11377−11384

OPb_4 tetrahedra can be viewed as derivatives from the continuous sheet of OPb_4 tetrahedra from the tetragonal modification of PbO compound. In compound **1**, two Br atoms are attached to the chain at the opposite position rotating the two pairs of edge-sharing OPb_4 tetrahedra, while the other type of Br atoms do not play the role of rotation, resulting in the $_\infty^1[OPb_2]$ chains constructed by finite linear zweier chains with four tetrahedra via the opposite edges. From single $_\infty^1[OPb_2]$ chains to $_\infty^1[O_2Pb_3]$ ribbons, the space is larger enough to locate three Br atoms instead of one BO_3 group, resulting in the layered structure of compound **2**. The infrared spectra of the title compounds are consistent with the crystallographic study. UV−vis−NIR diffuse reflectance spectroscopy suggests that the band gap of compound **2** is smaller than that of compound **1**. Finally, the TG-DSC curves suggest that compound **1** melts congruently and that compound **2** melts incongruently.

■ ASSOCIATED CONTENT

Supporting Information

Crystal data (CIF file); selected bond lengths (Å); scheme showing the substructures of $B2O_3$ group; coordinated environment of the Pb atoms; the infinite $_\infty^1[OPb_3B]$ chains; IR spectra for $Pb_2(O_4Pb_8)(BO_3)_3Br_3$ and $Pb_2(O_8Pb_{12})(BO_3)_2Br_6$, respectively. This material is available free of charge via the Internet at http://pubs.acs.org. [CCDC reference numbers 940246 and 940245 for $Pb_2(O_4Pb_8)(BO_3)_3Br_3$ and $Pb_2(O_8Pb_{12})(BO_3)_2Br_6$, respectively.]

■ AUTHOR INFORMATION

Corresponding Author

*(S.P.) E-mail: slpan@ms.xjb.ac.cn.

Notes

The authors declare no competing financial interest.

■ ACKNOWLEDGMENTS

This work is supported by 973 Program of China (Grant No. 2012CB626803), the National Natural Science Foundation of China (Grant Nos. U1129301, 51172277, 21101168, and 11104344), Main Direction Program of Knowledge Innovation of CAS (Grant No. KJCX2-EW-H03-03), The Funds for Creative Cross & Cooperation Teams of CAS, Major Program of Xinjiang Uygur Autonomous Region of China during the 12th Five-Year Plan Period (Grant No. 201130111), the High Technology Research & Development Program of Xinjiang Uygur Autonomous Region of China (Grant No. 201116143), and the Science and Technology Project of Urumqi (Grant No. G121130002).

■ REFERENCES

(1) (a) Yakubovich, O. V.; Yakovleva, E. V.; Golovanov, A. N.; Volkov, A. S.; Volkova, O. S.; Zvereva, E. A.; Dimitrova, O. V.; Vasiliev, A. N. *Inorg. Chem.* **2013**, *52*, 1538−1543. (b) Wu, H. P.; Yu, H. W.; Yang, Z. H.; Hou, X. L.; Su, X.; Pan, S. L.; Poeppelmeier, K. R.; Rondinelli, J. M. *J. Am. Chem. Soc.* **2013**, *135*, 4215−4218. (c) Chen, M. C.; Wu, L. M.; Lin, H.; Zhou, L. J.; Chen, L. *J. Am. Chem. Soc.* **2012**, *134*, 6058−6060. (d) Dong, X. Y.; Wu, H. P.; Shi, Y. J.; Yu, H. W.; Yang, Z. H.; Zhang, B. B.; Chen, Z. H.; Yang, Y.; Huang, Z. J.; Pan, S. L.; Zhou, Z. X. *Chem.—Eur. J.* **2013**, *19*, 7338−7341.

(2) (a) Krivovichev, S. V.; Mentré, O.; Siidra, O. I.; Colmont, M.; Filatov, S. K. *Chem. Rev.* **2013**, *113*, 6459−6535. (b) Bergerhoff, G.; Paeslack, J. *Z. Kristallogr.* **1968**, *126*, 112−123. (c) Carré, D.; Guitard, M.; Jaulmes, S.; Mazurier, A.; Palazzi,, M.; Pardo, M. P.; Laurelle, P.; Flahaut, J. *J. Solid State Chem.* **1984**, *55*, 287−292. (d) Krivovichev, S. V.; Siidra, O. I.; Nazarchuk, E. V.; Burns, P. C.; Depmeier, W. *Inorg. Chem.* **2006**, *45*, 3846−3848. (e) Nadir, S.; Swinnea, J. S.; Steinfink, H. *J. Solid State Chem.* **1999**, *148*, 295−301.

(3) (a) Krivovichev, S. V.; Filatov, S. K. *Am. Mineral.* **1999**, *84*, 1099−1106. (b) Krivovichev, S. V.; Shuvalov, R. R.; Semenova, T. F.; Filatov, S. K. *Z. Kristallogr.* **1999**, *214*, 135−138. (c) Latrach, A.; Mentzen, B. F.; Bouix, J. *Mater. Res. Bull.* **1985**, *20*, 853−860. (d) Pertlik, F. *Mineral. Petrol.* **1987**, *36*, 85−92.

(4) Krivovichev, S. V.; Armbruster, T.; Depmeier, W. *J. Solid State Chem.* **2004**, *177*, 1321−1332.

(5) (a) Ter Haar, G. L.; Bayard, M. A. *Nature* **1971**, *232*, 553−554. (b) Post, J.; Buseck, P. R. *Environ. Sci. Technol.* **1985**, *19*, 682−685. (c) Davis, A.; Drexler, J. W.; Ruby, M. V.; Nicholson, A. *Environ. Sci. Technol.* **1993**, *27*, 1415−1425.

(6) Matsumoto, H.; Miyake, T.; Iwahara, H. *Mater. Res. Bull.* **2001**, *36*, 1177−1184.

(7) (a) Dudnik, E. F.; Kolesov, I. S. *Sov. Phys. Solid State* **1980**, *22*, 700−701. (b) Kiosse, G. A.; Dudnik, E. F.; Sushko, S. A.; Kolesov, I. S. *Sov. Phys. Crystallogr.* **1982**, *27*, 713−714.

(8) (a) Toda, K.; Watanabe, S. *J. Appl. Phys.* **1995**, *77*, 2786−2791. (b) Yu, H. W.; Pan, S. L.; Wu, H. P.; Zhao, W. W.; Zhang, F. F.; Li, H. Y.; Yang, Z. H. *J. Mater. Chem.* **2012**, *22*, 2105−2110.

(9) (a) Behm, H. *Acta Crystallogr., Sect. B: Struct. Sci.* **1983**, *39*, 1317−1319. (b) Colmont, M.; Huvé, M.; Mentré, O. *Inorg. Chem.* **2006**, *45*, 6612−6621. (c) Bonhomme, F.; Alam, T. M.; Celestian, A. J.; Tallant, D. R.; Boyle, T. J.; Cherry, B. R.; Tissot, R. G.; Rodriguez, M. A.; Parise, J. B.; Nyman, M. *Inorg. Chem.* **2005**, *44*, 7394−7402. (d) Chen, X.; Song, F.; Chang, X.; Zang, H.; Xiao, W. *J. Solid State Chem.* **2009**, *182*, 3091−3097.

(10) Belokoneva, E. L.; Kabalov, Y. K.; Dimitrova, O. V.; Stefanovich, S. Y. *Z. Kristallogr.* **2003**, *48*, 49−53.

(11) Dong, L. Y.; Pan, S. L.; Wu, H. P.; Su, X.; Yu, H. W.; Wang, Y.; Chen, Z. H.; Huang, Z. J.; Yang, Z. H. *J. Solid State Chem.* **2013**, *204*, 64−69.

(12) Lima-de-Faria, J.; Hellner, E.; Liebau, F.; Mackovicky, E.; Parthé, E. *Acta Crystallogr., Sect. A: Found. Crystallogr.* **1990**, *46*, 1−11.

(13) Smith, D. K.; Roberts, A. C.; Bayliss, P.; Liebau, F. *Am. Mineral.* **1998**, *83*, 126−132.

(14) (a) Krivovichev, S. V.; Filatov, S. K. *Z. Kristallogr.* **1998**, *213*, 316−318. (b) Starova, G. L.; Krivovichev, S. V.; Filatov, S. K. *Z. Kristallogr.* **1998**, *213*, 650−653. (c) Siidra, O. I.; Krivovichev, S. V.; Armbruster, T.; Depmeier, W. *Z. Kristallogr.* **2008**, *223*, 204−211.

(15) Cheary, R. W.; Coelho, A. A. *J. Appl. Crystallogr.* **1992**, *25*, 109−121.

(16) *SAINT*, version 4.05, Program for Area Detector Absorption Correction; Siemens Analytical X-ray Instruments: Madison, WI, 1995.

(17) Blessing, R. H. *Acta Crystallogr., Sect. A* **1995**, *51*, 33−38.

(18) Sheldrick, G. M. *SHELXTL*, version 6.12; Bruker Analytical X-ray Instruments, Inc.: Madison, WI, 2001.

(19) (a) Shi, Y. J.; Pan, S. L.; Dong, X. Y.; Wang, Y.; Zhang, M.; Zhang, F. F.; Zhou, Z. X. *Inorg. Chem.* **2012**, *51*, 10870−10875. (b) Feng, K.; Shi, Y. G.; Yin, W. L.; Wang, W. D.; Yao, J. Y.; Wu, Y. C. *Inorg. Chem.* **2012**, *51*, 11144−11149.

(20) Spek, A. L. *J. Appl. Crystallogr.* **2003**, *36*, 7−13.

(21) (a) Brese, N. E.; O¢Keeffe, M. *Acta Crystallogr., Sect. B: Struct. Sci.* **1991**, *47*, 192−197. (b) Brown, I. D.; Altermatt, D. *Acta Crystallogr., Sect. B: Struct. Sci.* **1985**, *41*, 244−247. (c) Krivovichev, S. V.; Brown, I. D. *Z. Kristallogr.* **2001**, *216*, 245−247.

(22) (a) Kubelka, P.; Munk, F. *Tech. Phys.* **1931**, *12*, 593−601. (b) Tauc, J. *Mater. Res. Bull.* **1970**, *5*, 721−730.

(23) (a) Maggard, P. A.; Nault, T. S.; Stern, C. L.; Poeppelmeier, K. R. *J. Solid State Chem.* **2003**, *175*, 27−33. (b) Kozin, M. S.; Aliev, A.; Colmont, M.; Mentre, O.; Siidra, O. I.; Krivovichev, S. V. *J. Solid State Chem.* **2013**, *199*, 56−61.

(24) (a) Krivovichev, S. V.; Burns, P. C. *Z. Crystallogr.* **2003**, *218*, 357−365. (b) Li, Y. P.; Krivovichev, S. V.; Burns, P. C. *J. Solid State Chem.* **2000**, *153*, 365−370.

(25) (a) Li, J.; Xia, S.; Gao, S. *Spectrochim. Acta* **2005**, *433*, 196−198. (b) Zhou, G. H.; Ju, Z. J.; Wu, K. C.; Ye, N. *J. Mater. Chem.* **2012**, *22*,

1191−1198. (c) Yu, H. W.; Wu, H. P.; Pan, S. L.; Wang, Y.; Yang, Z. H.; Su, X. *Inorg. Chem.* **2013**, *52*, 5359−5365. (d) Wu, H. P.; Pan, S. L.; Poeppelmeier, K. R.; Li, H. Y.; Jia, D. Z.; Chen, Z. H.; Fan, X. Y.; Yang, Y.; Rondinelli, J. M.; Luo, H. S. *J. Am. Chem. Soc.* **2011**, *133*, 7786−7790.